PAPER

Theoretical and experimental investigation of model-free adaptive fuzzy sliding mode control for MRE based adaptive tuned vibration absorber

Theoretical and experimental investigation of model-free adaptive fuzzy sliding mode control for MRE based adaptive tuned vibration absorber

G N Susheelkumar, S M Murigendrappa⬤ and K V Gangadharan

Department of Mechanical Engineering, National Institute of Technology Karnataka, Surathkal, Mangalore-575025, India

E-mail: smm@nitk.ac.in

CrossMark

Abstract

In the present study, the performance of model-free adaptive fuzzy sliding mode control (AFSC) for the magnetorheological elastomer based adaptive tuned vibration absorber (MRE ATVA) has been investigated theoretically and experimentally. A room temperature vulcanized silicone rubber and Carbonyl iron particles form the constituents of MRE. Sliding mode and AFSCs have been developed. The boundary layer is applied for sliding surface to reduce chattering effect in the sliding mode control, in case of the AFSC, two fuzzy systems approximate the equivalent control and switching control. The Lyapunov theorem evaluates the asymptotical stability of the developed adaptive control based on fuzzy systems. The performance is compared for both the controls subjected to single frequency excitation. Further, the AFSC has been investigated for variable frequency excitation. The maximum reduction of transmissibility of primary mass is 38.14%. Based on the present study, the model-free AFSC is more effective in tuning the natural frequency of MRE ATVA by 0.5 s with parameter uncertainties and under variable frequency excitation as compared to the boundary layer sliding mode control.

Keywords: magnetorheological elastomer, vibration absorber, model-free, sliding mode control, fuzzy system, adaptive control

(Some figures may appear in colour only in the online journal)

1. Introduction

Vibration causes severe issues in machine tools, civil structures and aerospace vehicles [1]. To attenuate the effects of vibrations, vibration absorbers are employed on the dynamic systems. Based on their working principles, vibration absorbers are classified as passive, semi-active and active [2]. Passive vibration absorbers offer a simple solution to the vibration attenuation. However, due to their inherent constant properties, passive absorbers work only for a narrow frequency range. Furthermore, its performance deteriorates with varying operating frequencies. Active vibration absorber follows a more sophisticated approach where an opposite force is applied to suppress the disturbances of the vibrating

system. Though it provides an excellent solution for the mitigation of vibration, it suffers from drawbacks such as higher power consumption, sophisticated design and is best suitable for flexible structures. Semi-active vibration absorber overcomes the issues associated with both passive and active vibration absorbers. It is similar to the traditional passive vibration absorber, however with variable spring and damping properties, the semi-active absorbers effectively operate for a wider frequency range. Further, the power consumption is less in comparison with its active counterparts [3]. To achieve the variable spring and damping properties, several researchers have investigated for suitable smart materials such as shape memory alloy [4], magnetorheological fluid [5, 6] and magnetorheological elastomer (MRE) based materials
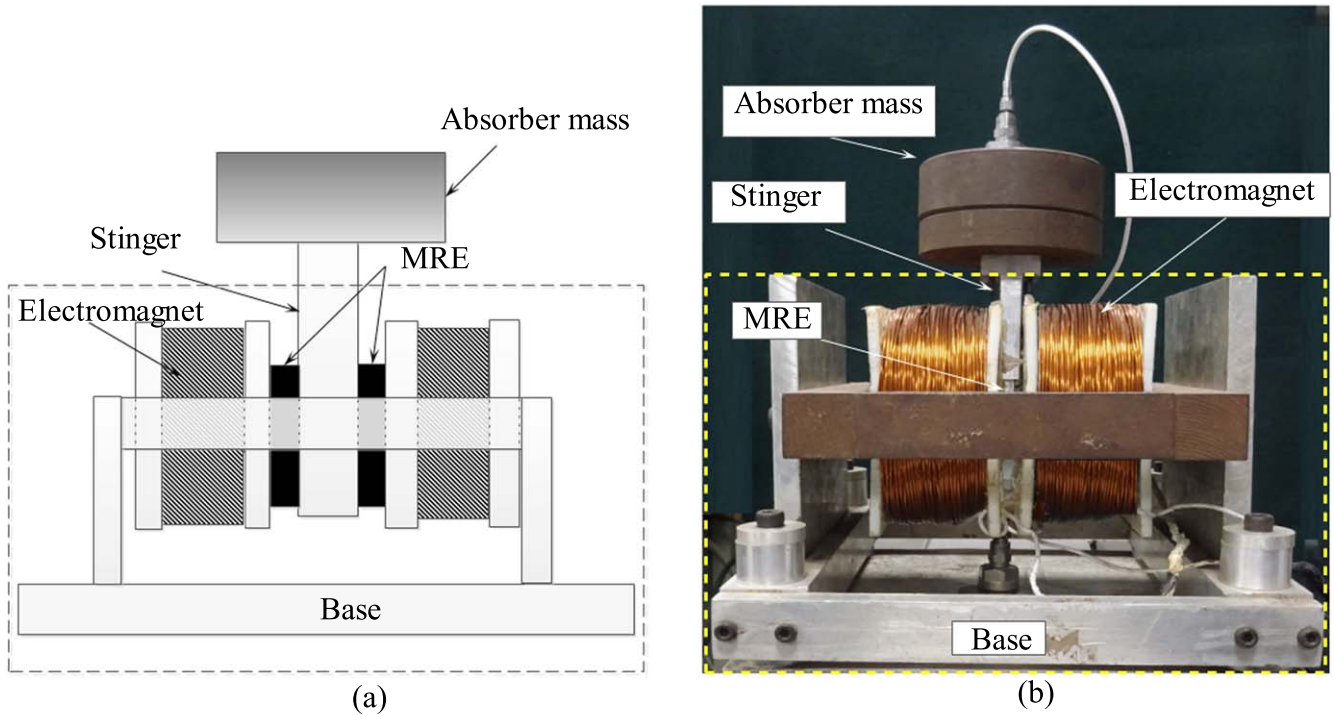
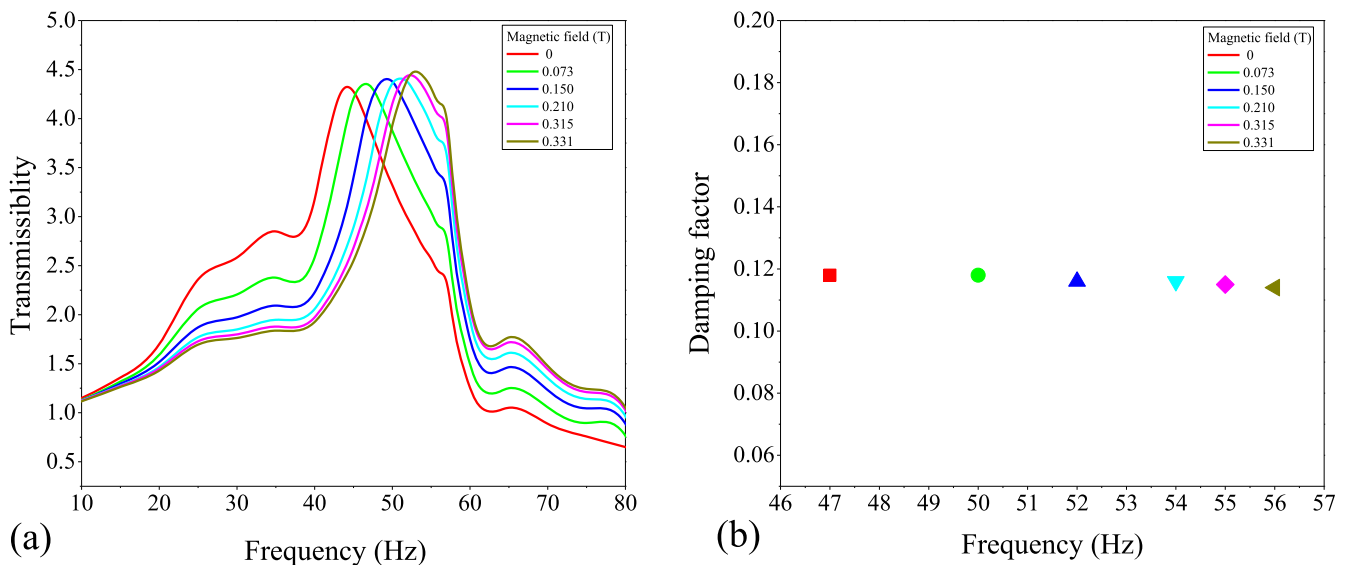**Figure 1.** MRE ATVA: (a) schematic and (b) photograph.

Figure 2. Plots of frequency shift of MRE ATVA: (a) transmissibility versus frequency and (b) damping factor versus frequency.

[7–10], with its variable dynamic properties, MRE has been found to be a potential material in semi-active vibration absorber. MRE is a composite material, consisting of a viscoelastic matrix with reinforcing iron particles. It changes its dynamic properties under the influence of a magnetic field. This field-dependent variations in the dynamic stiffness of the MRE can be effectively implemented in the semi-active dynamic vibration absorbers [11] resulting in magnetorheological elastomer adaptive tuned vibration absorber (MRE ATVA). The objective of the controllers, in general, is to rapidly tune natural frequency of the MRE ATVA with the excitation frequency to reduce the vibrations of the primary system [3]. At higher strain amplitude, nonlinearity and uncertainties exist in the MRE, which makes it difficult to tune the natural frequency of the MRE ATVA with excitation frequency [12, 13]. This necessitates the use of robust or adaptive control to tune the natural frequency of MRE ATVA. Much work has been carried out on fabrication, characterization [14–16] and modelling [17, 18] of MRE based smart structures. However, less research has been reported for MRE based smart structures with control strategies [13]. Liao *et al* [19] investigated the developed MRE based vibration isolator for tunable stiffness and damping properties and implemented ON–OFF control for the random

Table 1. Dynamic properties of MRE ATVA for variable magnetic field.

Current (A)	Voltage (V)	Magnetic field (T)	Frequency (Hz)	Stiffness (N m^{-1})	Damping Co-efficient (N s m^{-1})	Damping factor
0	0	0	47	136 916.2	109.41	0.118
0.5	5.32	0.073	50	154 952.7	116.40	0.118
1	10.64	0.150	52	167 596.9	119.00	0.116
1.5	15.96	0.210	54	180 736.9	123.58	0.116
2	21.23	0.315	55	187 492.8	124.48	0.115
2.5	26.6	0.331	56	194 372.7	125.95	0.114
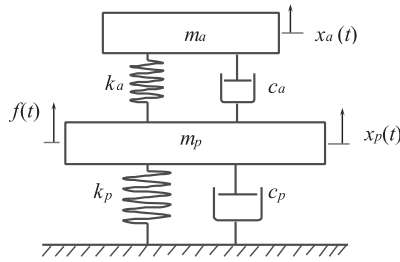
Figure 3. Schematic of dynamic vibration absorber.

base excitation of 2.5–18.75 Hz for vibration reduction. Behrooz *et al* [20] designed a model based Lyapunov control for an MRE isolator to suppress the vibration of a three-storey structure. Though the ON–OFF control and the Lyapunov control have been well explored, there are some issues associated with their implementation. The ON–OFF control is simple and can be effectively used in the actual implementation to the system. However, its oscillatory response limits its applications. On the other hand, the Lyapunov controls need an accurate model of the MRE and it is challenging to obtain a precise model of the MRE systems [21]. Fu *et al* [21] developed model-free fuzzy control for MRE vibration isolation system with a frequency shift of 107.3–187.3 Hz and a reduction of transmissibility of 54.4%. Nguyen *et al* [22] studied modelling of the MRE base isolator for seismic excitation and analysed the performance of fuzzy control. A shift frequency of 2.5 Hz with a maximum reduction of 30% in the amplitudes was reported. The Fuzzy logic control possesses certain advantages such as model-free, robustness and universal approximation theorem. Nevertheless, it lacks in methodical design, stability analysis and high computational load due to a larger number of fuzzy rules. The performance of semi-active system also depends on how quickly it can tune the natural frequency of the vibration absorber with excitation frequency. Xu *et al* [23] studied the performance of two-stage control strategies based on the lookup table and step size optimization. However, the two-stage control strategy takes a long time to tune the natural frequency of semi-active dynamic vibration absorber due to coarse and fine-tuning process. Liu *et al* [24] developed the autotuning algorithm methods to coincide the natural frequency of tunable vibration absorber with the excitation frequency. Results show one of the proposed methods takes more than 15 s to tune the natural frequency of the tunable vibration absorber accurately. Liao *et al* [3] investigated the

Phase-based stiffness tuning control algorithm for the MRE dynamic vibration absorber. The developed model-free algorithm tunes the natural frequency of MRE dynamic vibration absorber precisely in 4 s. The problems associated with the controllers as mentioned above can be overcome by integrating the fuzzy system with sliding mode control [25].

The present paper focuses on the design and analysis of sliding mode control and model-free adaptive fuzzy sliding mode control (AFSC) for MRE adaptive tuned vibration absorber (MRE ATVA). The sliding mode control is a non-linear controller, and it is very effective even with disturbance present in a system. But the conventional sliding mode control has a chattering issue associated with discontinuous control output. This chattering can be overcome by providing the boundary layer along the sliding surface. The discontinuous control output can be effectively smoothened with a continuous function which is enclosed by a boundary layer [26–28]. The proposed AFSC combines the sliding mode, fuzzy logic, and adaptive control. The adaptive fuzzy controls are used to approximate the control terms namely, the equivalent control and switching control. Even with non-linearity and parameter uncertainties of MRE ATVA, the proposed control quickly and precisely tunes the natural frequency of the MRE ATVA.

2. MRE based adaptive tuned vibration absorber

The developed adaptive tuned vibration absorber device based on MRE has been discussed in the following sections.

2.1. Preparation of MRE

The constituents of the anisotropic MRE include room temperature vulcanization based silicone rubber (Performance Polymers, MoldSil 102LL with CAT 9) with Carbonyl iron particles (BASF, Type CN, Average diameter 5 μm) as its filler material. Volume fraction of the iron particles is 27%. The MRE sample is prepared with thorough mixing of silicone rubber and carbonyl iron. Silicone oil is added to the mixture about 10% of weight to reduce the zero-field stiffness of MRE. The prepared mixture is poured into a mould of size 25 × 25 × 3 mm and degassed in a vacuum chamber. Further, the sample is cured for 24 h at room temperature, 24 °C with 0.7 T magnetic field to obtain the anisotropic MRE.
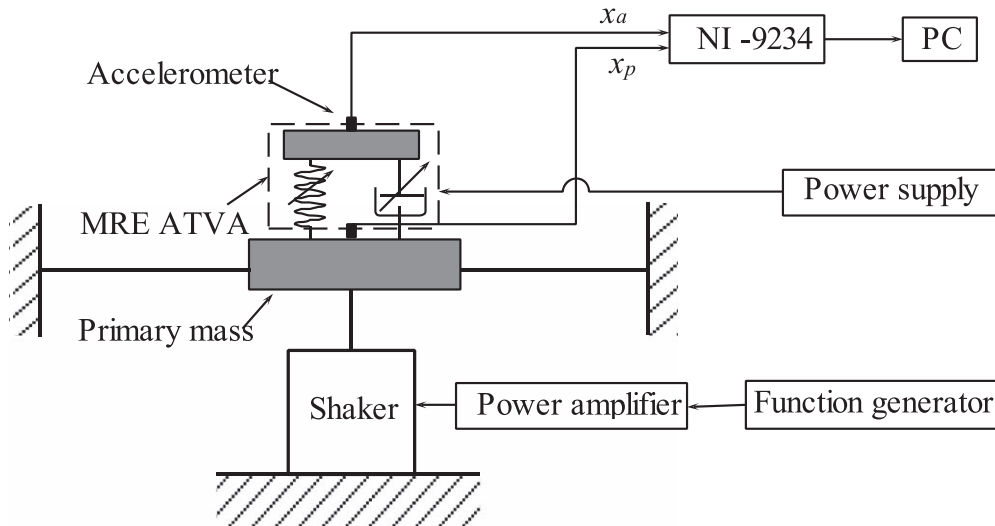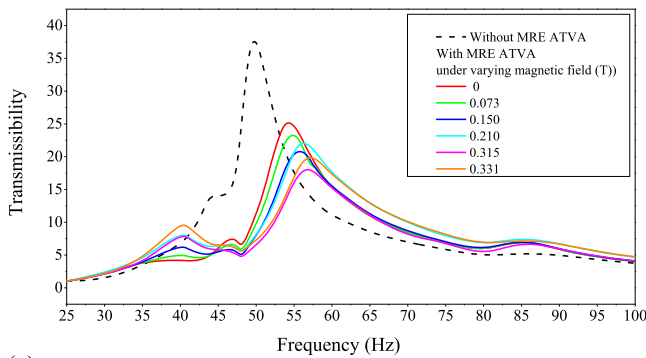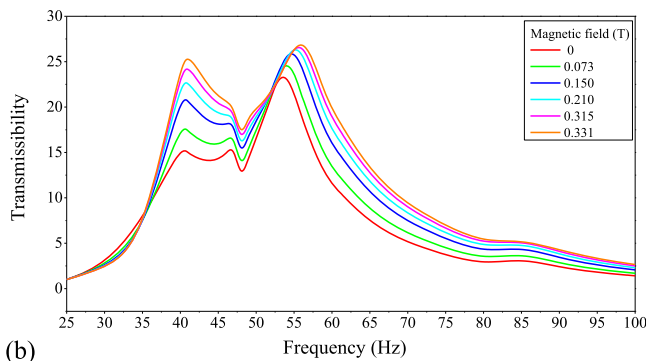
Figure 4. Schematic of combined system (primary mass and MRE ATVA).

Figure 5. Plot of transmissibility versus frequency: (a) primary mass and (b) MRE ATVA.
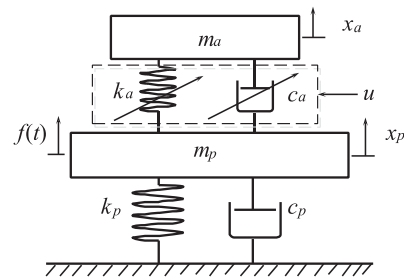

Figure 6. Schematic of MRE ATVA with control.

the magnetic field of 0.66 T is achieved with the current of 5 A.

2.3. Frequency shift of MRE ATVA

To extract the dynamic properties of the MRE ATVA, it is subjected to steady state excitation from 10 to 80 Hz in step of 1 Hz at constant input acceleration. The peak amplitude of each frequency is recorded. The field dependent variations in the transmissibility and damping factor with varying frequencies are plotted as shown in figure 2. It is observed that the natural frequency of the MRE ATVA increases from 47 to 56 Hz under the magnetic field of 0.315 T. The increase in the natural frequency as shown in figure 2(a) is attributed to the field-dependent increase in the stiffness of the MRE under the influence of the magnetic field. In the presence of a magnetic field, the carbonyl iron particles align themselves in the direction of the applied field. This results in the formation of magnetic dipoles between adjacent carbonyl iron particles which induces compressive forces on the interlaying matrix, increasing in the stiffness of MRE [3, 11, 14]. It is also observed from figure 2(b) that there is no significant variation in the damping factor with variable magnetic field [29]. The field dependent properties of MRE ATVA are presented in table 1.

2.2. Fabrication of MRE ATVA

Figure 1 shows the developed MRE ATVA. It consists of two MRE samples arranged to act in a double shear mode with a mass of 1.57 kg. The MRE samples are fixed between the absorber mass and the electromagnet as shown in figure 1(a). The electromagnet consists of a copper wire of wire gauge AWG18. The number of turns is 2400 with an inductance of 153 mH and a resistance, 10.2 Ω. The magnetic field is controlled with an external DC power supply. For electromagnet,
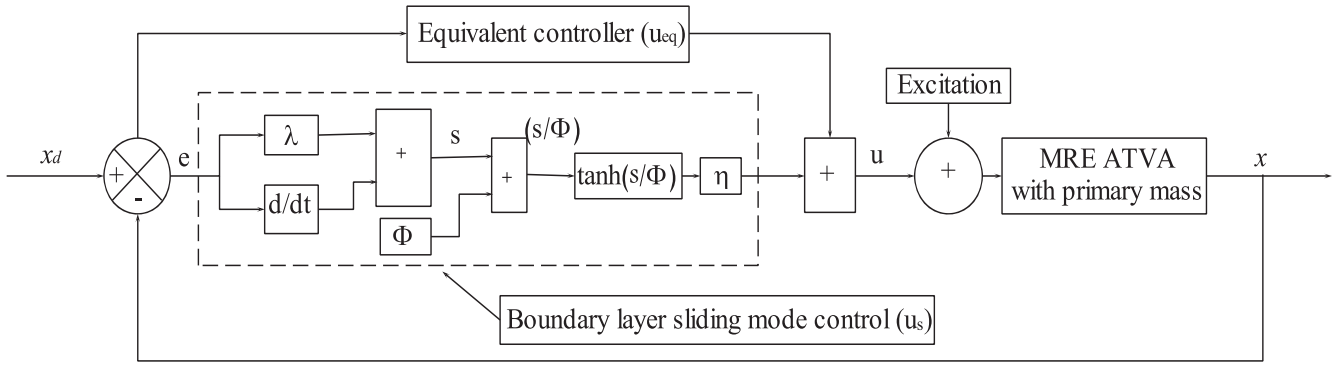
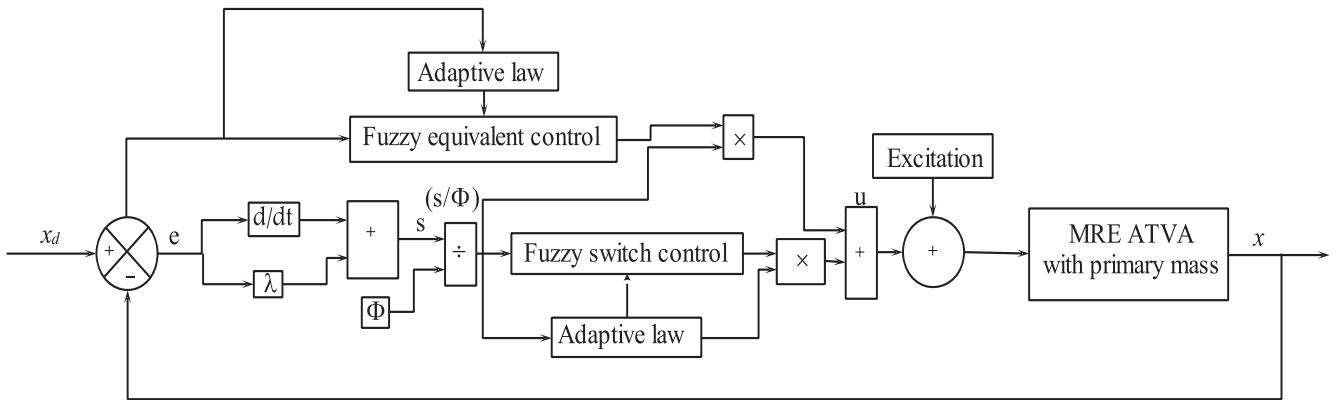**Figure 7.** Schematic of boundary layer sliding mode control.

Figure 8. Schematic of adaptive fuzzy sliding mode control.

3. Transmissibility of combined (primary mass and MRE ATVA) system

Figure 3 illustrates the schematic of dynamic vibration absorber is subjected to a steady state excitation force, $f(t) = F_0 \sin(\omega t)$.

The governing differential equations of dynamic vibration absorber are given as

$$m_p \ddot{x}_p(t) + k_p x_p(t) + c_p \dot{x}_p + k_p \times (x_p(t) - x_a(t)) + c_p(\dot{x}_p(t) - \dot{x}_a(t)) = f(t) \quad (1)$$

where, m, k and c are the mass, stiffness and damping coefficient, respectively. $x(t)$ represents the displacement of the mass at a given time, t. The suffixes, p and a correspond to the primary mass and absorber, respectively [30].

Assuming, the general solutions for equations (1) and (2) as [31].

$$x_p = X_p e^{i\omega t} \quad (3)$$

$$x_a = X_a e^{i\omega t}. \quad (4)$$

The amplitudes of vibration are given

$$X_p = \frac{[(k_a - m_a\omega^2) + c_a\omega j]F_0}{[(k_p - m_p\omega^2)(k_a - m_a\omega^2) - m_a k_a\omega^2] + [k_p - (m_p + m_a)\omega^2)c_a\omega]j} \quad (5)$$

$$X_a = \frac{[k_a + c_a\omega j]F_0}{[(k_p - m_p\omega^2)(k_a - m_a\omega^2) - m_a k_a\omega^2] + [k_p - (m_p + m_a)\omega^2)c_a\omega]j}, \quad (6)$$

$$m_a \ddot{x}_a(t) + k_a(x_a(t) - x_p(t)) + c_p(\dot{x}_a(t) - \dot{x}_p(t)) = 0, \quad (2)$$

where, ω, the excitation frequency and j is the complex variable.

The static displacement of the primary mass is given by

$$X_{st} = \frac{F_0}{k}. \tag{7}$$

The transmissibility of the primary mass and absorber is obtained by dividing the equations (5) and (6) from (7), yields.

$$\frac{X_p}{X_{st}}$$
$$= \sqrt{\frac{(2\zeta r)^2 + (r^2 - \beta^2)^2}{(2\zeta r)^2(r^2 - 1 + \mu r^2) + [\mu r^2\beta^2 - (r^2 - 1)(r^2 - \beta^2)]^2}} \tag{8}$$

$$\frac{X_a}{X_{st}}$$
$$= \sqrt{\frac{(2\zeta r)^2 + \beta^4}{(2\zeta r)^2(r^2 - 1 + \mu r^2) + [\mu r^2\beta^2 - (r^2 - 1)(r^2 - \beta^2)]^2}}, \tag{9}$$

where, the natural frequency of absorber, $\omega_a = \sqrt{\frac{k_a}{m_a}}$, the natural frequency of the primary mass without absorber, $\omega_p = \sqrt{\frac{k_p}{m_p}}$, frequency ratio, $r = \frac{\omega}{\omega_p}$, ratio of natural frequencies, $\beta = \frac{\omega_a}{\omega_p}$, mass ratio, $\mu = \frac{m_a}{m_p}$, and ζ is the damping factor.

The schematic of experimental set-up of the combined system is as shown in figure 4. It consists of a primary mass and MRE ATVA. The primary mass of 9.35 kg and MRE based ATVA is mounted at the centre of the massless beam with fixed-fixed end conditions. A mass ratio of 0.18 is maintained between the primary and the absorber mass. An electromagnetic shaker (Make: Vibration Test System; Type VTS-80) is used to excite the combined system through a power amplifier (Make: Techron; Type 5507). Input frequencies are generated through a function generator (Make: Agilent; Type 33220A). Accelerometers (Make: Kistler; Type K-shear) are mounted on the primary and the absorber mass to measure the accelerations signals. The signals are acquired using a data acquisition module (National Instruments, Type NI-9234) which is further processed using LabVIEW (Version -2017). The magnetic field is induced in the electromagnet via a DC power supply (Make: Ametek; Type XG150-5.6).

Field dependent variations in the peak accelerations are obtained for the combined system under steady-state sweep from 25 to 100 Hz at constant input acceleration. Figure 5 depicts the measured transmissibility of primary mass and MRE ATVA. The natural frequency of primary mass without MRE ATVA is 50 Hz. It is observed that the natural frequency of primary mass shifts to two new component frequencies with the addition of the MRE ATVA. Further, the maximum amplitudes of the primary mass decrease with an increase in the magnetic field.

4. Control strategies

To apply the MRE ATVA in real-time conditions, the controls are essential to regulate the induced magnetic field to the electromagnet. The following section illustrates the design and analysis of controls for the MRE ATVA.
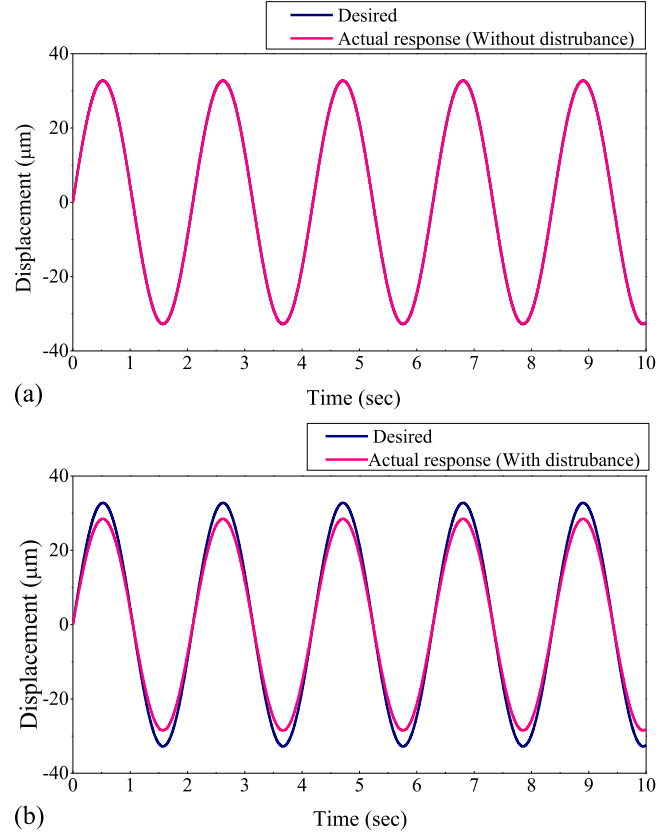

Figure 9. Time response of boundary sliding mode control: (a) position tracking without disturbance and (b) position tracking with disturbance.

4.1. Boundary layer sliding mode control (BSMC)

Sliding mode control is a robust nonlinear control. It has an equivalent control term and a sliding mode control term, which provides stability and robustness to the system with parameter uncertainties [32].

The dynamic governing equation of primary mass with the parameter uncertainties, external disturbance, and control input as shown in figure 6 is given by

$$m_p\ddot{x}_p + k_p x_p + c_p\dot{x}_p + k_p(x_p - x_a) + c_p(\dot{x}_p - \dot{x}_a) = u + dt, \tag{10}$$

where, u is the control input, and dt is the time-dependent disturbance with known upper bond, D, i.e. $|dt| \leqslant D$.

By rearranging the equation (10), we have, the acceleration of the primary mass as

$$\ddot{x}_p = f(x, t) + u + dt, \tag{11}$$

where, $f(x, t) = -m_p^{-1}(k_p x_p + c_p\dot{x}_p + k_a(x_p - x_a) + c_a(\dot{x}_p - \dot{x}_a))$. The total control input of the MRE ATVA, u is expressed as

$$u = u_{eq} + u_s, \tag{12}$$

where u_{eq} is the equivalent control and u_s is the switching control
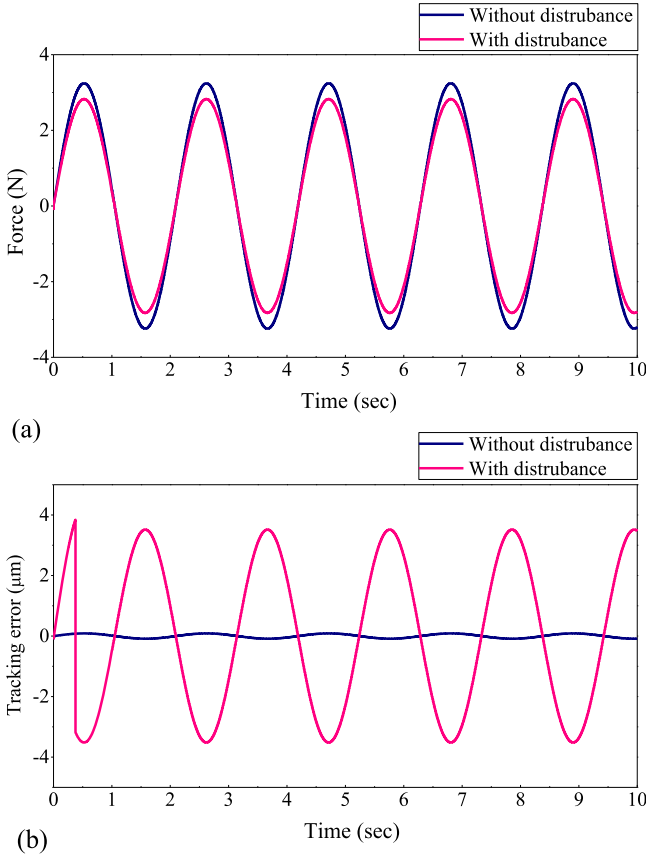
(a)

(b)

Figure 10. Time response of boundary sliding mode control: (a) force and (b) tracking error.

(a)

(b)

(c)

Figure 11. Time response of (a) position tracking of adaptive fuzzy sliding mode control with disturbance, (b) force with disturbance and (c) tracking error with disturbance.

The sliding surface s is defined as,

$$s = -\lambda e - \dot{e}, \tag{13}$$

where error signal, e represents the difference between desired, x_{pd} and actual displacement, x_p of primary mass, i.e. $e = (x_{pd} - x_p)$ and λ is the positive constant. The objective of the sliding mode control is to ensure the error, $e = 0$. This can be guaranteed by forcing the state trajectory towards the sliding surface [33].

Differentiating equation (13) with respect to time, t and utilizing the equation (11) and e yields,

$$\dot{s} = -\lambda \dot{e} - \ddot{x}_{pd} + f(x,\ t) + u + dt. \tag{14}$$

To attain the desired state trajectory without considering uncertainty and disturbance the equivalent control, u_{eq} is determined by equating equation (14) to zero. Thus, we have,

$$u_{eq} = \lambda \dot{e} + \ddot{x}_{pd} - f(x, t) - dt. \tag{15}$$

However, to attain the desired state trajectory with disturbances or uncertainties in the system, the equivalent control effort, u_{eq} do not confirm better performance and leads to instability. Therefore, the auxiliary control must be considered to stabilize system [27]. The total control with auxiliary control is given by
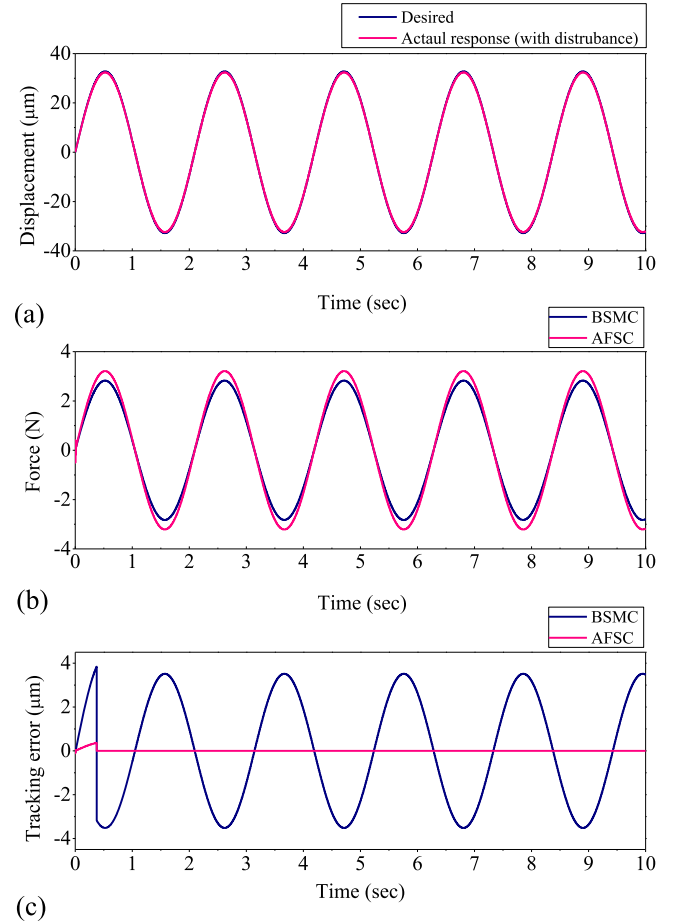
$$u = \lambda \dot{e} + \ddot{x}_{pd} - f(x, t) + u_s, \tag{16}$$

where, $u_s = -\eta \text{sign}(s)$ and η is the positive constant.

The zero error for the state trajectory with disturbances or uncertainties in the system is ensured with the following condition.

$$s\dot{s} = s\, u_s = s\,[-\eta \text{sign}(s)] = -\eta |s| \leqslant 0. \tag{17}$$

Sliding mode control is a discontinuous control in which chattering is inherently present and leads to fluctuation in the control output. The boundary layer method is considered to reduce the chattering effect. Further, the discontinuous function changes to smooth saturation function near to a significant region of the switching surface. The relation for the boundary layer is given by [28]

$$B(t) = \{x:\ |s(x, t)| \leqslant \Phi\}, \tag{18}$$

where, Φ is the boundary layer thickness.

With the inclusion of the boundary layer, the total control input as shown in figure 7 can be expressed as,

$$u = \lambda\dot{e} + \ddot{x}_{pd} - f(x, t) - \eta sat(s/\Phi), \quad (19)$$

where, the saturation function is given by [33]

$$sat\left(\frac{s}{\Phi}\right) = \begin{cases} \tanh\left(\frac{s}{\Phi}\right), & for \left|\frac{s}{\Phi}\right| \geqslant 1 \\ \frac{s}{\Phi}, & for \left|\frac{s}{\Phi}\right| \leqslant 1 \end{cases}. \quad (20)$$

4.2. Fuzzy logic system

In general, the fuzzy system works on the principle of universal approximation theorem [34], and any nonlinear function can be approximated by use of fuzzy systems. A fuzzy system consists of fuzzy if-then rules and is expressed as

$$R^{(j)}: \text{ If } x_1 \text{ is } F_1^j \text{ and } x_n \text{ is } F_n^j \text{ then } y \text{ is } B^j, \quad (21)$$

where x_1 and y are input and out variables. F_1^j and B^j fuzzy sets. With centre-average defuzzification, product inference and single value fuzzification, the output of the fuzzy is written as [25],

$$y(x) = \frac{\sum_{j=1}^{l} y^j \left(\prod_{i=1}^{n} \mu_{F_i^j}(x_i)\right)}{\sum_{j=1}^{l} \prod_{i=1}^{n} \mu_{F_i^j}(x_i)}, \quad (22)$$

where $\mu_{F_i^j}(x_i)$ is the membership function of the input variable x_i and y^l represents a crisp value at which the membership function μ_{Bj} for fuzzy output set reaches its maximum value which is assumed as $\mu_{Bj}(y^i = 1)$.

By introducing the concept of fuzzy basic function $\xi(x)$, the output of the fuzzy system is given by [28]

$$y(x) = \theta^T \xi(x), \quad (23)$$

where, $\theta = (y^1, ..., y^l)^T$, $\xi(x) = (\xi^1(x), ..., \xi^l(x))^T$ and

$$\xi^j(x) = \frac{\prod_{i=1}^{n} \mu_{F_i^j}(x_i)}{\sum_{j=1}^{l} \prod_{i=1}^{n} \mu_{F_i^j}(x_i)}. \quad (24)$$

The fuzzy membership functions for the equivalent control is given by

$$\mu_{NM}(x_i) = \exp-\left(\frac{x_i + \pi/6}{\pi/24}\right)^2,$$

$$\mu_{NS}(x_i) = \exp-\left(\frac{x_i + \pi/12}{\pi/24}\right)^2,$$

$$\mu_Z(x_i) = \exp-\left(\frac{x_i}{\pi/12}\right)^2,$$

$$\mu_{PS}(x_i) = \exp-\left(\frac{x_i - \pi/12}{\pi/24}\right)^2 \text{ and }$$

$$\mu_{PM}(x_i) = \exp-\left(\frac{x_i - \pi/6}{\pi/24}\right)^2$$

and also, the membership functions of switching control is given by

$$\mu_N(s) = \frac{1}{1 + \exp(5(s + 3))}$$

$$\mu_Z(s) = \exp(-s^2) \text{ and }$$

$$\mu_P(s) = \frac{1}{1 + \exp(-5(s - 3))}.$$

To approximate the equivalent control $\hat{f}(x|\theta_f)$ and switching control $\hat{h}(s|\theta_h)$ for MRE ATVA with parameter uncertainties and variable frequency excitation, the total of 20 fuzzy rules are considered.

4.3. Adaptive fuzzy sliding mode control (AFSC)

The developed control in equation (19) does not work if the upper bound of $f(x, t)$ and dt are unknown, for which the fuzzy systems are used to approximate $f(x, t)$ and $\eta sign(s/\Phi)$ as $\hat{f}(x|\theta_f)$ and $\hat{h}(s|\theta_h)$ as shown in figure 8.

The total control input of the AFSC is given by

$$u = \lambda\dot{e} + \ddot{x}_{pd} - \hat{f}(x|\theta_f) - \hat{h}(s|\theta_h), \quad (25)$$

where

$$\hat{f}(x|\theta_f) = \theta_f^T \xi(x) \text{ and } \hat{h}(s|\theta_h) = \theta_h^T \phi(s).$$

To define the optimal parameters of the fuzzy system, the following conditions should satisfy.

$$\theta_f^* = \arg\min_{\theta_f \in \Omega_f}\left[\sup_{x \in R^n}|\hat{f}(x|\theta_f) - f(x, t)|\right] \quad (26)$$

$$\theta_h^* = \arg\min_{\theta_h \in \Omega_h}\left[\sup_{x \in R^n}|\hat{h}(s|\theta_h) - \eta sign(s/\Phi)|\right], \quad (27)$$

where Ω_f and Ω_h are constraint sets for θ_f and θ_h, respectively

The minimum approximation error is given by

$$\omega = f(x, t) - \hat{f}(x|\theta_f). \quad (28)$$

Considering the equation (14)

$$\dot{s} = -\lambda\dot{e} - \ddot{x}_{pd} + f(x, t) + u + dt \quad (29)$$

$$= f(x, t) - \hat{f}(x, t) - \hat{h}(s) + dt \quad (30)$$

$$= \hat{f}(x|\theta_f^*) - \hat{f}(x, t) + f(x, t)$$
$$\quad - \hat{f}(x|\theta_f^*) + \hat{h}(s|\theta_h^*) \quad (31)$$
$$\quad - \hat{h}(s) - \hat{h}(s|\theta_h^*) + dt$$

$$= \hat{f}(x|\theta_f^*) - \hat{f}(x, t) + \hat{h}(s|\theta_h^*)$$
$$\quad - \hat{h}(s) + \omega - \hat{h}(s|\theta_h^*) + dt \quad (32)$$

$$= \varphi_f^T \xi(x) + \varphi_h^T \phi(s) + dt + \omega - \hat{h}(s|\theta_h^*), \quad (33)$$

where $\varphi_f = \theta_f - \theta_f^*$ and $\varphi_h = \theta_h - \theta_f^*$.

Now consider Lyapunov function candidate of the form

$$V = \frac{1}{2}s^2 + \frac{1}{2\gamma_1}\varphi_f^T\varphi_f + \frac{1}{2\gamma_2}\varphi_h^T\varphi_h, \quad (34)$$

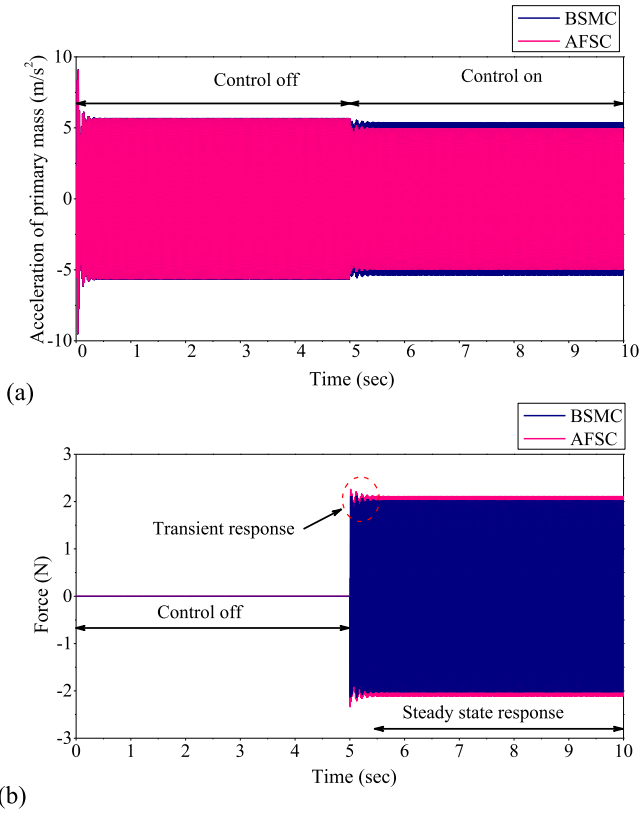where γ_1 and γ_2 are positive constants. The time derivative of

Figure 12. Simulated responses at 50 Hz: (a) acceleration of primary mass and (b) force.

Figure 13. Simulated responses at 52 Hz: (a) acceleration of primary mass and (b) force.
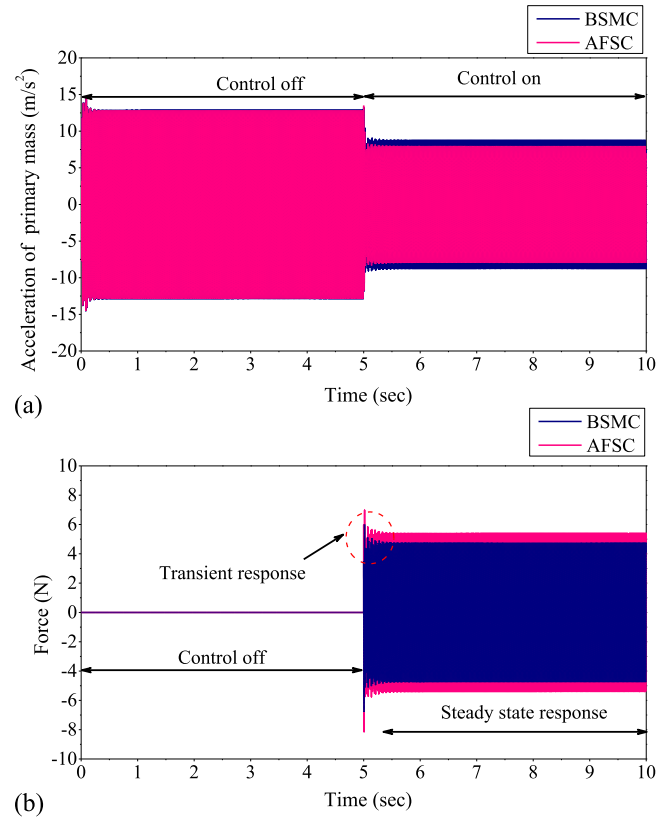

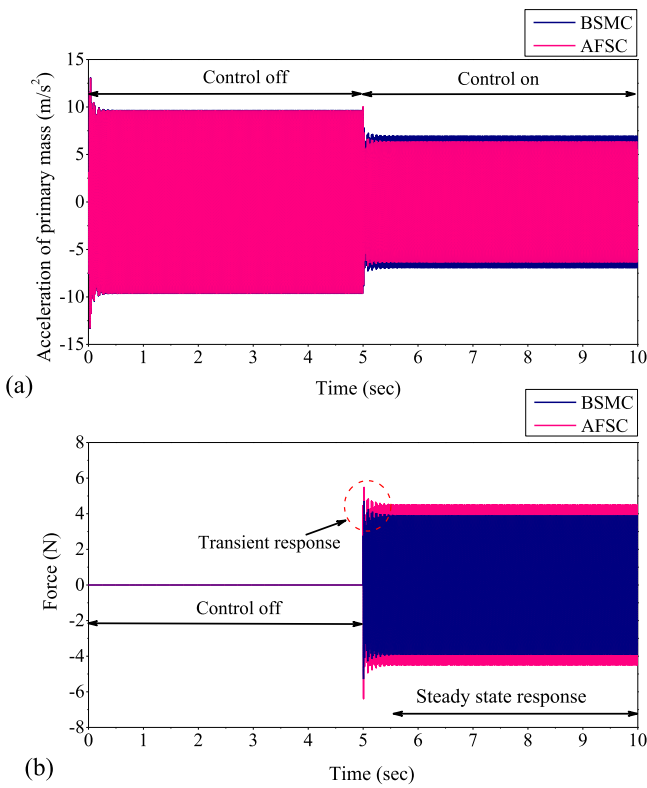**Figure 14.** Simulated responses at 54 Hz: (a) acceleration of primary mass and (b) force.
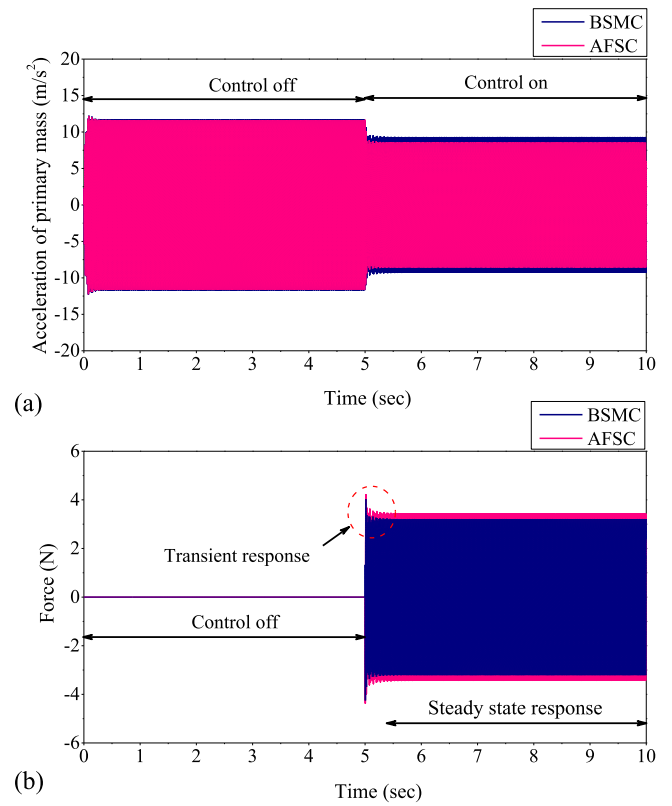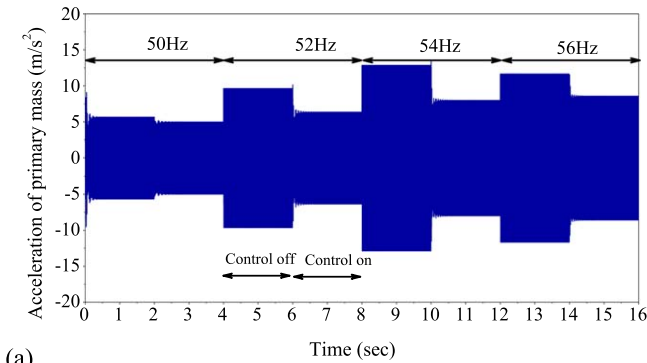

Figure 15. Simulated responses at 56 Hz: (a) acceleration of primary mass and (b) force.

Table 2. Simulation results of the acceleration of primary mass under different frequencies and controls.

| Frequency (Hz) | Without control | With controls | | | | | | | | |
| | | BSMC | | | | AFSC | | | | |
	$\ddot{x}_p$(m s^{-2})	η	$\ddot{x}_p$(m s^{-2})	% of decrease	Force (N)	γ_1	γ_2	$\ddot{x}_p$(m s^{-2})	% of decrease	Force (N)
50	5.67	38	5.33	5.99	2.01	45	55	4.98	12.16	2.10
52	9.61	153	6.89	28.3	3.88	53	170	6.33	34.13	4.46
54	12.84	152	8.70	32.24	4.74	56	175	7.97	37.92	5.38
56	11.49	35	9.18	14.62	3.02	52	60	8.58	25.53	3.41

η-Gain of the sliding mode control, γ_1-Adaptive gain of fuzzy equivalent control and γ_2-Adaptive gain of fuzzy switching control.
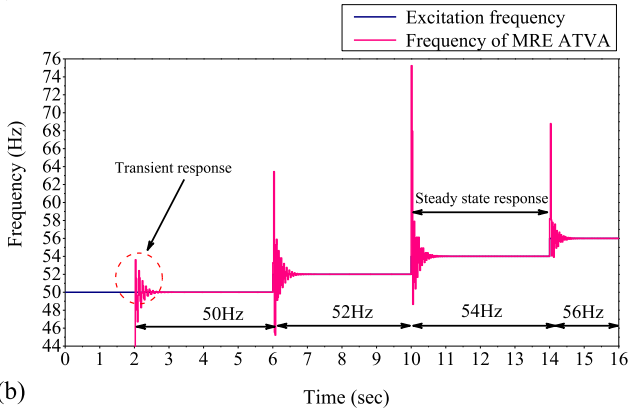
Figure 16. Simulated responses at variable frequency excitation: (a) acceleration of primary mass and (b) frequency of MRE ATVA.

V is given by

$$\dot{V} = s\dot{s} + \frac{1}{\gamma_1}\varphi_f^T\dot{\varphi}_f + \frac{1}{\gamma_2}\varphi_h^T\dot{\varphi}_h \quad (35)$$

$$= s(\varphi_f^T\xi(x) + \varphi_h^T\phi(s) + dt + \omega - \hat{h}(s|\theta_h^*)) + \frac{1}{\gamma_1}\varphi_f^T\dot{\varphi}_f + \frac{1}{\gamma_2}\varphi_h^T\dot{\varphi}_h \quad (36)$$

$$= s\varphi_f^T\xi(x) + \frac{1}{\gamma_1}\varphi_f^T\dot{\varphi}_f + s\varphi_h^T\phi(s) + \frac{1}{\gamma_2}\varphi_h^T\dot{\varphi}_h + s(dt - \hat{h}(s|\theta_h^*) + s\omega \quad (37)$$

Table 3. Simulation results of transmissibility of primary mass under variable frequency excitation with AFSC.

| Frequency (Hz) | Without control | With control | |
| | Transmissibility | AFSC | |
		Transmissibility	% of decrease
50	11.26	9.75	13.41
52	19.08	12.37	35.16
54	25.49	16.18	36.49
56	22.82	17.29	24.23

$$\dot{V} \leqslant s\varphi_f^T\xi(x) + \frac{1}{\gamma_1}\varphi_f^T\dot{\varphi}_f + s\varphi_h^T\phi(s) + \frac{1}{\gamma_2}\varphi_h^T\dot{\varphi}_h + sdt - s(D + \eta_\Delta sign(s)) + s\omega. \quad (38)$$

Finally, the time derivative of Lyapunov function candidate, we have

$$\dot{V} < \frac{1}{\gamma_1}\varphi_f^T\gamma_1 s\xi(x) + \dot{\varphi}_f + \frac{1}{\gamma_2}\varphi_h^T(\gamma_2 s\phi(s) + \dot{\varphi}_h) + s\omega - |s|\eta, \quad (39)$$

where $\dot{\varphi}_f = -\dot{\theta}_f = \gamma_1 s\xi(x)$, $\dot{\varphi}_h = -\dot{\theta}_h = -\gamma_2 s\phi(s)$ are the adaptive laws.

Simplification of equation (39) yields

$$\dot{V} \leqslant s\omega - |s|\eta \leqslant 0. \quad (40)$$

With fuzzy approximation, the minimum approximation error, ω can be achieved with the adaptive fuzzy system. Equation (40) implies that $\dot{V}$ is negative semidefinite and all the signals of the control are bounded. The error signal, $e(t)$ is bounded for all values of time t. To prove asymptotic stability of the tracking error, i.e. $e(t) \to 0$ and the sliding surface, $s(t) \to 0$ as time, $t \to \infty$. Defining $|s| \leqslant \eta_\Delta$, [35] equation (40) can be written as

$$\dot{V} \leqslant |s||\omega| - |s|\eta \leqslant \eta_\Delta|\omega| - |s|\eta. \quad (41)$$

Integrating equation (40) on both sides, we have

$$\int_0^\tau |s|\,d\tau \leqslant \frac{1}{\eta}(|V(0)| + |V(t)|) + \frac{\eta_\Delta}{\eta}\int_0^\tau |\omega|\,d\tau. \quad (42)$$
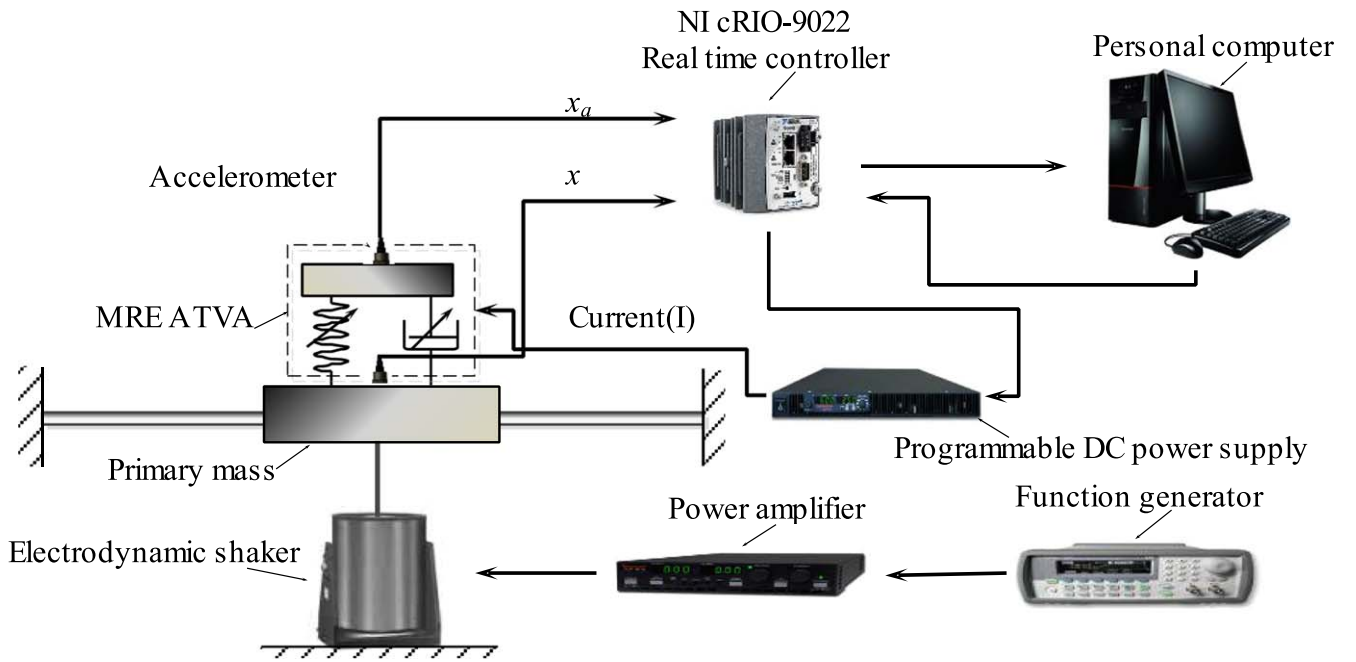
Figure 17. Schematic of setup of real-time controller.
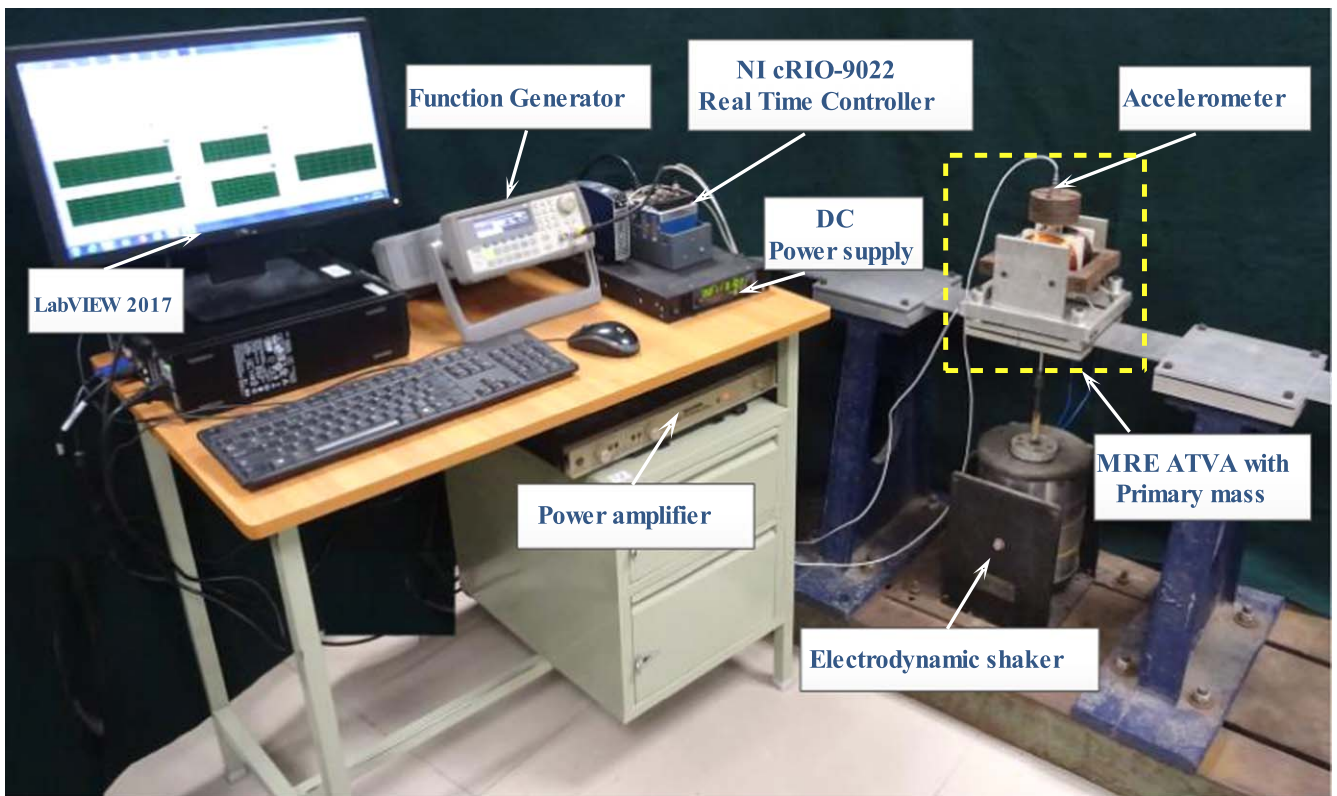
Figure 18. Photograph of experimental setup of real-time controller.

The sliding surface is thus, $s \in L_1$. From the equation (40) it is known that derivative of sliding surface, $\dot{s}(t)$ bounded and $s(t)$ is uniformly continuous. From the corollary of Barbalat's lemma [36] we have, $s(t) \rightarrow 0$ and $e(t) \rightarrow 0$ as $t \rightarrow \infty$.

5. Simulation analysis

The simulation analysis has been carried out to investigate the performance of proposed controllers. The developed controls are simulated in MATLAB Simulink.

**Table 4.** The experimental result of the acceleration of primary mass under different frequencies and controls.

| Frequency (Hz) | Without control | With controls | | | | | | | | | |
| | | BSMC | | | | AFSC | | | | | |
	$\ddot{x}_p$(m s^{-2})	η	$\ddot{x}_p$(m s^{-2})	% of decrease	Control voltage (V)	γ_1	γ_2	$\ddot{x}_p$(m s^{-2})	% of decrease	Control voltage (V)
52	9.35	150	7.53	19.40	8.43	55	170	7.35	21.31	10.5
54	12.77	156	8.70	31.81	13.58	52	179	8.36	34.51	16.29
56	11.22	40	7.09	36.82	18.48	56	65	6.73	40.04	21.70

η-Gain of the sliding mode control, γ_1-Adaptive gain of fuzzy equivalent control and γ_2-Adaptive gain of fuzzy switching control.
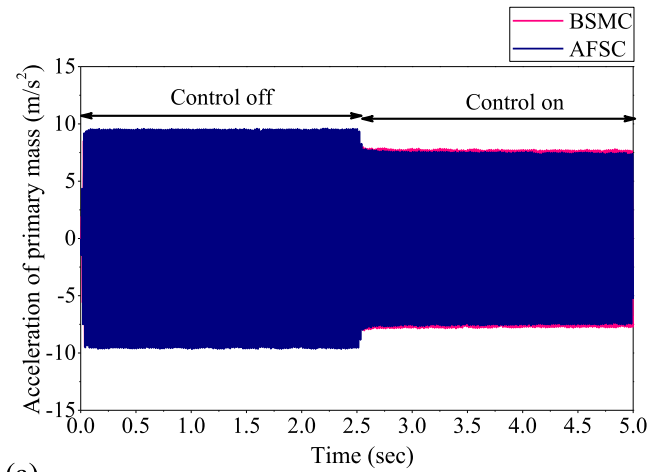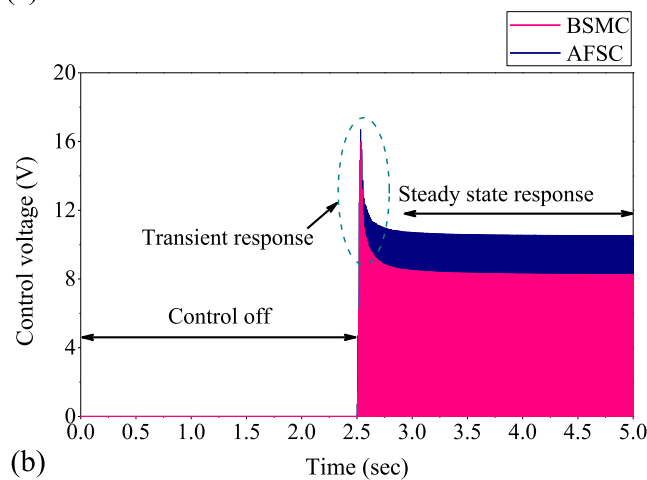
Figure 19. Measured responses at 52 Hz: (a) acceleration of primary mass and (b) control voltage.
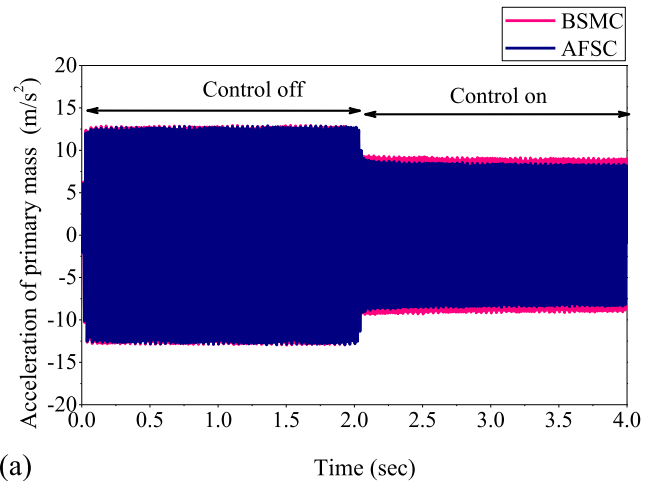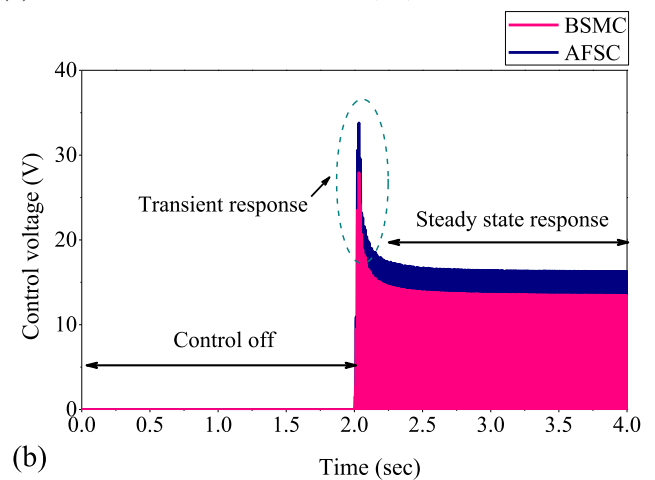

Figure 20. Measured responses at 54 Hz: (a) acceleration of primary mass and (b) control voltage.

5.1. Position tracking of MRE ATVA

For the simulation, the parameters considered in this study for the primary system are: mass $m_p = 9.35$ kg, stiffness, $k_p = 922808.011$ N m^{-2}, damping coefficient, $c_p = 37.64$ N s m^{-2}, and for MRE ATVA the parameters are: mass, $m_a = 1.57$ kg, stiffness, $k_a = 136\,916.2$ N m^{-2} damping coefficient, $c_a = 109.41$ N s m^{-2}. Performance of both controls is verified without and with disturbance conditions. The control parameters of BSMC are $\lambda = 1200$, $\Phi = 0.3$ and $\eta = 50$ and for the AFSC the parameters are $\gamma_1 = 1590$ and $\gamma_2 = 1580$.

Figure 9 depicts the time response of BSMC without and with disturbance. The control tracks the desired signal precisely as shown in figure 9(a) without disturbance. However, as the disturbance introduced in the system, the performance of the BSMC deteriorates, which is observed from the time response as shown in figure 9(b) with a noticeable difference between the desired signal and the actual response of the system. Figures 10(a) and (b) shows the response of control force and tracking error of MRE ATVA without and with disturbance. As the disturbance is induced in the system, the input control force decreases where as the error between the desired signal
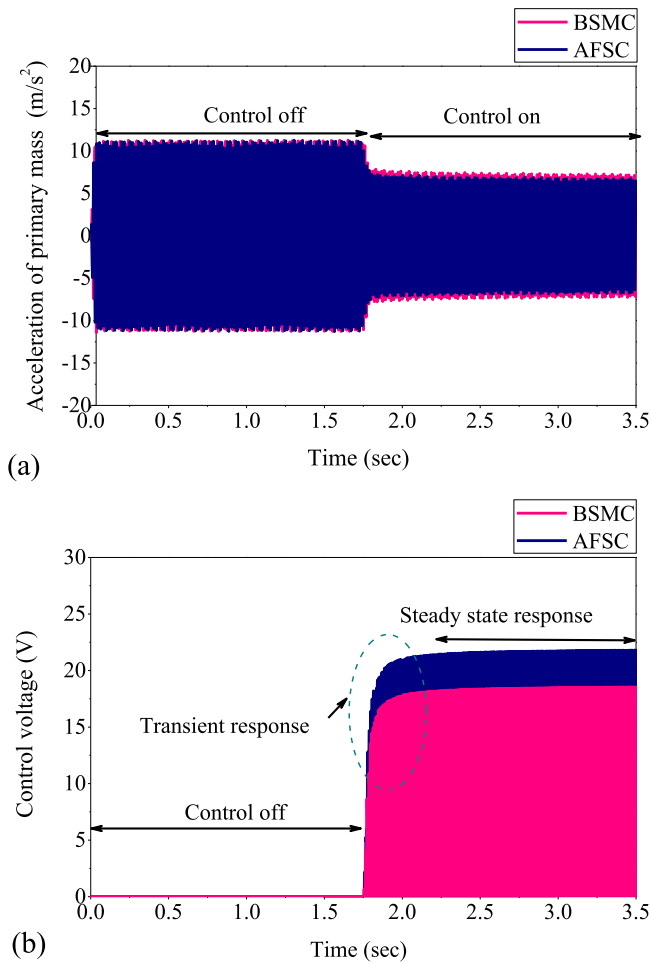
Figure 21. Measured responses at 56 Hz frequency: (a) acceleration of primary mass and (b) control voltage.

Figure 22. Measured responses under variable frequency excitation: (a) acceleration of primary mass, (b) control voltage and (c) FFT.

and the actual response increases. Figure 11 depicts the performance of AFSC with the external disturbance induced in MRE ATVA. The actual signal tracks the desired signal with minimal error is as shown in figure 11(a). This highlights the adaptive nature of the AFSC. Figure 11(b) and (c) show the response of control force and tracking error of BSMC and AFSC, respectively, for the MRE ATVA with disturbance.

5.2. Simulation of single frequency excitation

The simulation of both BSMC and AFSC for MRE ATVA with primary mass has been carried out for single frequency excitation from 50 to 56 Hz in steps of 2 Hz as shown in figures 12–15. Figure 12 depicts the simulated time response of primary mass for frequency excitation at 50 Hz. The time response of primary mass for both the controls are as shown in figure 12(a). For the first 5 s, the system is excited at a constant frequency of 50 Hz keeping both the controls in OFF condition. Under this condition, the computed acceleration of the primary mass, 5.67 m s^{-2}. For next 5 s, the combined system is excited with the controls in ON condition and the computed accelerations of primary mass for BSMC and AFSC controls are 5.33 m s^{-2} and 4.98 m s^{-2}, respectively. The percentage reduction of amplitudes of acceleration for BSMC and AFSC in comparison with control in OFF
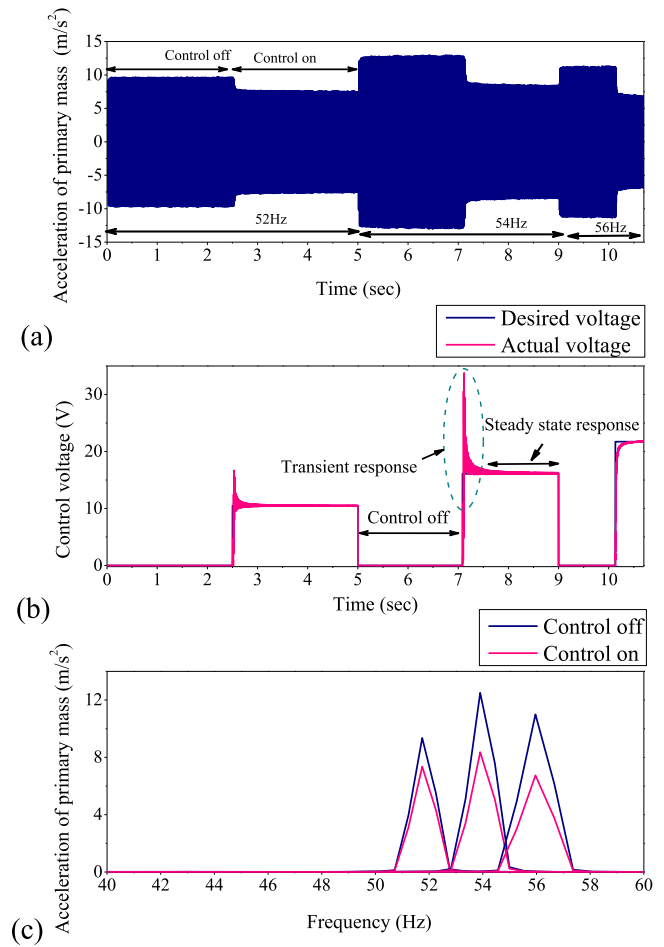
Table 5. Experimental results of transmissibility of primary mass under variable frequency excitation with AFSC.

| Frequency (Hz) | Without control | With control | |
| | | AFSC | |
	Transmissibility	Transmissibility	% of decrease
52	18.56	14.98	19.25
54	25.21	17.03	32.43
56	24.23	14.99	38.14

condition are 5.99 and 12.16, respectively. Figure 12(b) shows the input control force of MRE ATVA. The amplitudes of BSMC and AFSC computed as 2.01 N and 2.10 N, respectively. In case of ON condition of the control, the response of the control input is divided into two parts, the transient response, and steady state response. However, the transient response for both controls is less than 0.5 s whereas, the steady state error for both the controls differs significantly with disturbances in MRE ATVA. This confirms that the AFSC is more effective in reducing the amplitude of acceleration of primary mass compared to BSMC. Similar behaviour is observed for all the remaining excitation frequencies considered in the present study as in figures 13–15

and the results are summarized in table 2. It is also observed that the percentage reduction of acceleration amplitude of the primary mass is higher at 50 and 56 Hz and lower at 52 and 54 Hz.

5.3. Simulation of variable frequency excitation

It is observed from the equation (19) that the BSMC works only for a single frequency excitation. With the instantaneous change in the excitation frequency, the developed control needs to tune to the natural frequency of MRE ATVA. This incapability of the conventional BSMC is resolved by incorporating the fuzzy systems to the existing control which forms the AFSC as referred in equation (25). Figure 16 depicts the simulated time response of AFSC. Figure 16(a) shows the acceleration response of the primary mass with variable frequency excitation. The combined system is excited from 50 to 56 Hz with an increment of 2 Hz. Each of the frequencies is excited for 4 s with a time period of control OFF condition for 2 s and remaining 2 s for ON condition. Figure 16(b) depicts the tracking of the natural frequencies of the ATVA with the excitation frequencies. The tuning of the ATVA frequencies with the variable frequency excitation takes place with the minimum transient response of less than 0.5 s. As the excitation frequency increases, both the overshoot and the time of transient response decreases significantly. The simulated transmissibility of the primary mass under variable frequency excitation, with and without control is summarized in table 3.

6. Experimental setup for real-time controller

The developed BSMC and AFSC are implemented on Compact RIO Real-time controller (Make National Instruments; Type cRIO-9022). The input module (NI-9234) and output module (NI-9264) are mounted on real-time controller. The acceleration signals are acquired using an input module which is further processed using LabVIEW (Version-2017) on a real-time platform. The voltage output module is used to control the magnetic field induced in the electromagnet via a DC power supply (AMETEK, XG150-5.6, Programmable power supply). Figures 17 and 18 illustrates schematic and photograph of real-time controller setup.

7. Experimental analysis

7.1. Experiment of single frequency excitation

The experimental response of primary mass for all the frequencies are as shown in figures 19–21. Figure 20(a) presents the measured acceleration of the primary mass at a frequency of 54 Hz. The excitation of the system is carried out for 4 s, and the acceleration of the primary mass is recorded. In the absence of control, the measured amplitude of acceleration of primary mass, 12.77 m s^{-2}. With the implementation of the developed controls, the acceleration amplitudes of the primary mass for BSMC and AFSC reduces to 8.70 m s^{-2} and 8.76 m s^{-2}, respectively, with an overall percentage reduction of 31.81% and 34.57%,

respectively. Figure 20(b) shows the control voltage of the electromagnet. The plot shows a measured input control voltage of 13.58 and 16.29 V for the BSMC and AFSC, respectively. Transient response for both the controls is observed as 0.5 s, after it attains the steady state response. The results obtained by simulation for both controls follow a similar trend as that of the experimental results and demonstrates that the AFSC is more efficient in reduction of acceleration amplitude of primary mass. Similar performance is observed for all frequencies considered in the present investigation as presented in table 4.

7.2. Experiment of variable frequency excitation

Figure 22(a) presents the acceleration of primary mass for a variable frequency excitation from 52 to 56 Hz with an increment of 2 Hz. For the excitation period of 5 s with an excitation frequency of 52 Hz, the natural frequency of ATVA under OFF condition of the control is set for 47 Hz. With the control ON condition the natural frequency shifts to 52 Hz. Similarly, the combined system is excited for the frequencies of 54 Hz and 56 Hz with excitation time 4 and 2 s, respectively. The control is ON condition at excitation time of 7.2 and 10.2 s. This influences the shift of the natural frequencies of the MRE ATVA to 54 and 56 Hz. This confirms the effectiveness of AFSC to track the natural frequencies of MRE ATVA with excitation frequencies.

Figure 22(b) depicts the input control voltage to all excitation frequencies. The natural frequencies of the MRE ATVA are depend on the input control voltage of electromagnet. Figure 22(c) shows the FFT of all excitation frequencies with AFSC in OFF and ON conditions. The measured transmissibility of the primary mass under variable frequency excitation, with and without control is summarized in table 5.

8. Conclusions

In the present study, the performance of model-free AFSC for the MRE ATVA was investigated theoretically and experimentally. Experiment trials were carried out to extract the dynamic properties of MRE ATVA. The natural frequency of MRE ATVA shifts from 47 to 56 Hz under the magnetic field, 0.315 T. Sliding mode, and model-free AFSCs have been developed. The Lyapunov theorem evaluates the asymptotical stability of the developed adaptive control based on fuzzy systems. The performance was compared for both the controls subjected to single frequency excitation. Further, the AFSC was investigated for variable frequency excitation. The maximum reduction of transmissibility of primary mass was 38.14%. The model-free AFSC is found to be more effective in tuning the natural frequency of MRE ATVA in less than 0.5 s with parameter uncertainties and under variable frequency excitation as compared to the BSMC.

Acknowledgments

Ministry of Human Resources Development) and experimental facility provided by Centre for System Design (CSD): A Centre of Excellence (http://csd.nitk.ac.in/) at National Institute of Technology Karnataka, India.

ORCID iDs

S M Murigendrappa ⬤ https://orcid.org/0000-0002-4722-1615

References

[1] Deng H X and Gong X L 2007 Adaptive tuned vibration absorber based on magnetorheological elastomer *J. Intell. Mater. Syst. Struct.* **18** 1205–10

[2] Liao G J, Gong X L, Kang C J and Xuan S H 2011 The design of an active-adaptive tuned vibration absorber based on magnetorheological elastomer and its vibration attenuation performance *Smart Mater. Struct.* **20** 075015

[3] Liao G, Gong X and Xuan S 2014 Phase based stiffness tuning algorithm for a magnetorheological elastomer dynamic vibration absorber *Smart Mater. Struct.* **23** 015016

[4] Tai N T and Ahn K K 2011 Adaptive proportional-integral-derivative tuning sliding mode control for a shape memory alloy actuator *Smart Mater. Struct.* **20** 055010

[5] Khan I U, Wagg D and Sims N D 2016 Improving the vibration suppression capabilities of a magneto-rheological damper using hybrid active and semi-active control *Smart Mater. Struct.* **25** 085045

[6] Gu Z Q and Oyadiji S O 2008 Application of MR damper in structural control using ANFIS method *Comput. Struct.* **86** 427–36

[7] Sinko R, Karnes M, Koo J H, Kim Y K and Kim K S 2013 Design and test of an adaptive vibration absorber based on magnetorheological elastomers and a hybrid electromagnet *J. Intell. Mater. Syst. Struct.* **24** 803–12

[8] Komatsuzaki T, Inoue T and Terashima O 2016 Broadband vibration control of a structure by using a magnetorheological elastomer-based tuned dynamic absorber *Mechatronics* **40** 128–36

[9] Yang Z, Qin C, Rao Z, Ta N and Gong X 2014 Design and analyses of axial semi-active dynamic vibration absorbers based on magnetorheological elastomers *J. Intell. Mater. Syst. Struct.* **25** 2199–207

[10] Lerner A A and Cunefare K A 2008 Performance of MRE-based vibration absorbers *J. Intell. Mater. Syst. Struct.* **19** 551–63

[11] Poojary U R and Gangadharan K V 2017 Magnetic field and frequency dependent LVE limit characterization of magnetorheological elastomer *J. Braz. Soc. Mech. Sci. Eng.* **39** 1365–73

[12] Ying Z, Ni Y and Sajjadi M 2013 Nonlinear dynamic characteristics of magneto-rheological visco-elastomers *Sci. China Technol. Sci.* **56** 878–83

[13] Choi S B, Li W, Yu M, Du H, Fu J and Do P X 2016 State of the art of control schemes for smart systems featuring magneto-rheological materials *Smart Mater. Struct.* **25** 043001

[14] Poojary U R, Hegde S and Gangadharan K V 2016 Dynamic blocked transfer stiffness method of characterizing the magnetic field and frequency dependent dynamic viscoelastic properties of MRE *Korea Aust. Rheol. J.* **28** 301–13

[15] Popp K M, Kröger M, Li W, Zhang X Z and Kosasih P B 2010 MRE properties under shear and squeeze modes and applications *J. Intell. Mater. Syst. Struct.* **21** 1471–7

[16] Hegde S, Kiran K and Gangadharan K V 2015 A novel approach to investigate effect of magnetic field on dynamic properties of natural rubber based isotropic thick magnetorheological elastomers in shear mode *J. Cent. South Univ.* **22** 2612–9

[17] Liao G, Fu J, Li P and Yu M 2016 Neural network modeling of magneto-rheological elastomer isolator *2016 Chinese Control Decis. Conf. (28-30 May)* 2668–73

[18] Yu Y, Li Y C, Li J C, Gu X Y, Royel S and Pokhrel A 2016 Nonlinear and hysteretic modelling of magnetorheological elastomer base isolator using adaptive neuro-fuzzy inference system *Appl. Mech. Mater.* **846** 258–63

[19] Liao G J, Gong X L, Xuan S H, Kang C J and Zong L H 2012 Development of a real-time tunable stiffness and damping vibration isolator based on magnetorheological elastomer *J. Intell. Mater. Syst. Struct.* **23** 25–33

[20] Behrooz M, Wang X and Gordaninejad F 2014 Performance of a new magnetorheological elastomer isolation system *Smart Mater. Struct.* **23** 045014

[21] Fu J, Li P, Wang Y, Liao G and Yu M 2016 Model-free fuzzy control of a magnetorheological elastomer vibration isolation system: analysis and experimental evaluation *Smart Mater. Struct.* **25** 035030

[22] Nguyen X B, Komatsuzaki T, Iwata Y and Asanuma H 2018 Modeling and semi-active fuzzy control of magnetorheological elastomer-based isolator for seismic response reduction *Mech. Syst. Signal Process.* **101** 449–66

[23] Xu Z, Gong X and Chen X 2011 Development of a mechanical semi-active vibration absorber *Adv. Vib. Eng.* **10** 229–38

[24] Liu K, Liao L and Liu J 2005 Comparison of two auto-tuning methods for a variable stiffness vibration absorber *Trans. Can. Soc. Mech. Eng.* **29** 81–96

[25] Wang J, Rad A B and Chan P T 2001 Indirect adaptive fuzzy sliding mode control: I. Fuzzy switching *Fuzzy Sets Syst.* **122** 21–30

[26] Suryawanshi P V, Shendge P D and Phadke S B 2016 A boundary layer sliding mode control design for chatter reduction using uncertainty and disturbance estimator *Int. J. Dyn. Control* **4** 456–65

[27] Vijay M and Jena D 2017 PSO based neuro fuzzy sliding mode control for a robot manipulator *J. Electr. Syst. Inf. Technol.* **4** 243–56

[28] Wang J, Rad A B and Chan P T 2001 Indirect adaptive fuzzy sliding mode control: II. Fuzzy switching *Fuzzy Sets Syst.* **122** 21–30

[29] Yang J, Gong X, Deng H, Qin L and Xuan S 2012 Investigation on the mechanism of damping behavior of magnetorheological elastomers *Smart Mater. Struct.* **21** 125015

[30] Xu Z, Gong X, Liao G and Chen X 2010 An active-damping-compensated magnetorheological elastomer adaptive tuned vibration absorber *J. Intell. Mater. Syst. Struct.* **21** 1039–47

[31] Kumbhar S B, Chavan S P and Gawade S S 2018 Adaptive tuned vibration absorber based on magnetorheological elastomer-shape memory alloy composite *Mech. Syst. Signal Process.* **100** 208–23

[32] Vijay M and Jena D 2016 Intelligent adaptive observer-based optimal control of overhead transmission line de-icing robot manipulator *Adv. Robot.* **30** 1215–27

[33] Parameswaran A P, Ananthakrishnan B and Gangadharan K V 2015 Design and development of a model free robust controller for active control of dominant flexural modes of vibrations in a smart system *J. Sound Vib.* **355** 1–18

[34] Feng J, Gao Q, Guan W and Huang X 2017 Fuzzy sliding mode control for erection mechanism with unmodelled dynamics *Automatika* **58** 131–40

[35] Fei J and Xin M 2015 Adaptive fuzzy sliding mode control of MEMS gyroscope sensor using fuzzy switching approach *J. Dyn. Syst. Meas. Control* **137** 1479–84

[36] Ho H F, Wong Y K and Rad A B 2009 Adaptive fuzzy sliding mode control with chattering elimination for nonlinear SISO systems *Simul. Model. Pract. Theory* **17** 1199–210